In Situ XAS Study of CoB_i Modified Hematite Photoanodes

Lifei Xi,[a] Christoph Schwanke,[a] Dong Zhou,[b] Dorian Drevon,[a] Roel van de Krol[c] and Kathrin M. Lange[a,d*]

[a]Young Investigator Group Operando Characterization of Solar Fuel Materials (EE-NOC),[b] Department of Microstructure and Residual Stress Analysis, [c]Institute for Solar Fuels, Helmholtz-Zentrum Berlin für Materialien und Energie GmbH, 12489 Berlin, Germany, [d]Universität Bielefeld, Physikalische Chemie, Universitätsstr.25, D-33615 Bielefeld, Germany.

Corresponding Author

kathrin.lange@helmholtz-berlin.de

ABSTRACT

Solar water splitting is a potentially scalable method to store solar energy in the form of renewable hydrogen gas. In this study, we demonstrate that the photoelectrochemical (PEC) performance of hematite photoanodes can be improved by modification with the oxygen evolution catalyst CoB_i. The current density at 1.23 V of the pristine hematite under one sun is 0.88 mA cm^{-2} and increases to 1.12 mA cm^{-2} after CoB_i modification (~27% improvement). The presence of a CoB_i cocatalayst layer is proposed to improve oxygen evolution reaction (OER) kinetics and also to prevent electron-hole recombination at the surface via passivating surface defects as well as suppressing the tunneling of electrons from the hematite core, thus improving the photocurrents and resulting in a negative shift of photocurrent onset potentials. These effects of CoB_i modification are supported by experimental data obtained by electrochemical impedance spectroscopy (EIS), PEC and *incident photon-to-current* efficiency (IPCE) measurements. To investigate the electronic structure of the CoB_i cocatalyst deposited on hematite, XPS and *in situ* X-ray absorption spectroscopy (XAS) are employed. Co K-edge spectra under different potentials and light conditions are recorded. This makes the present work different from most of the previous works. Using a quantitative analysis method, the information on the mean oxidation state of Co in the CoB_i film under applied potential and illumination are revealed. We also compare different methods for determining the oxidation state from the edge position and find that the integral method and half height methods are best suitable. In summary, the present work underlines the improvement of the semiconductor/cocatalyst interface of oxygen evolving photoanodes and strengthens the importance of *in situ* XAS spectroscopy when studying catalysts. This study is the

first report so far combining the studies of PEC performance of a CoB_i modified hematite nanorod array photoanode and *in situ* XAS at the Co K-edge.

KEYWORDS: XAS, XANES, cobalt borate, *in situ*, hematite, photoanode, photoelectrochemistry, cocatalyst

Introduction

Solar water splitting is a potentially scalable method to store solar energy in the form of renewable hydrogen fuels.[1] The overall water splitting reaction is a thermodynamically uphill reaction (ΔG=237 KJ/mol) which is a multiple electron transfer process.[2] The oxygen evolution reaction (OER) has been recognized as one of the main bottlenecks for the conversion process due to its large requisite overpotential.[3] Hematite (α-Fe_2O_3) is a potentially interesting candidate due to its moderate band gap (E_g = ~2.2 eV), chemical stability, abundance and low cost.[4,5] Although respectable photocurrents of several mA/cm^2 have been achieved, the reported efficiencies of hematite are notoriously lower than the theoretical value, mainly due to the short lifetime of the photo-generated charge carriers (< 10ps) and concomitantly short hole diffusion length (2 - 4 nm).[6] One can (partially) solve this by adopting a nanostructured morphology, e.g., nanorods or nanowire arrays, ultrathin films, ultrathin films deposited on a three-dimensional nanophotonic structure[7] or core/shell structures.[8] However, then the slow water oxidation process limits the solar to fuel energy conversion efficiency. Modification of the photoanode with an OER catalyst improves the overall system efficiency, since it reduces the overpotential required for the OER to take place, and in some cases promotes separation and diffusion of carrier species.[9] The previously investigated cocatalysts for hematite include cobalt oxide (CoO_x),[10] cobalt phosphate (CoP_i), [7,11,12] nickel borate (NiB_i),[13] $Ni(OH)_2$,[14] IrO_2,[15] or Ru based catalysts.[16] For example, Zhong *et al.* deposited a Co^{2+} cocatalyst on the hematite photoanode using different preparation methods: photo-assisted electrodeposition of CoP_i, electrodeposition of CoP_i and Co^{2+} wet impregnation.[11] They found that the photo-assisted electrodeposition provides a more uniform distribution of CoP_i onto hematite than which is obtained by the electrodeposition or simple Co^{2+} wet impregnation, thus giving better performing photoanodes.[17] Hong *et al.* found that photochemical deposition of a NiB_i oxygen evolution catalyst (OEC) on hematite nanorods led to a cathodic shift of >200 mV in the onset potential for water oxidation and a 9.5 fold enhancement in the photocurrent density

at 0.86 V vs. RHE compared to the unmodified hematite photoanode.[13] In addition, there are some published works related to surface plasmonic effects, e.g., for gold nanoparticle decorated hematite photoelectrodes.[8,18] Previously we studied the oxygen evolution from hematite photoanodes.[19-21] We found that *in situ* incorporation of the OEC Co_3O_4 during hydrothermal growth of hematite nanorod arrays with 5% Co^{2+} added, which means that Co^{2+} is added with an initial molar ratio of Co^{2+} to Fe^{3+} of 1:20, can greatly improve the photocurrent and the *incident photon-to-current* efficiency (IPCE) of photoanodes.[19]

Recently, Farrow *et al.* found that with increasing film thickness, the cobalt borate (CoB_i) films were more active than CoP_i and ultimately displayed a significantly superior performance.[22] A very recent study showed that the activity of a CoB_i modified $SrTiO_3$ photoanode is superior to that of CoP_i under UV illumination.[23] They found that the higher water oxidation activity of the CoB_i results from the greater amount of cocatalyst present on the $SrTiO_3$ substrates, and thus more active OER sites during the photoelectrochemical (PEC) reaction. In that study, they mainly focused on the intensity change of Co K-edge spectra under *in situ* condition. Based on these findings, the catalytic activity of the cobalt based catalysts strongly depends on the preparation method and the supporting electrolyte. The development of a simple method for the modification of hematite photoanodes with cobalt based catalyst is thus desirable.

In this study the PEC performance under visible light illumination and the electronic structure and valence change of Co during solar water oxidation of CoB_i modified hematite nanorods are investigated using AM1.5 solar simulator and *in situ* X-ray absorption spectroscopy (XAS). As an element-specific probe, XAS provides the electronic information of each absorber atom contained in the material. XAS at the transition metal K-edge is a powerful technique for determining the mean oxidation states of materials.[24] Recent work showed that thin surface layer of CoP_i on substrate can be detected and studied via the Co K-edge.[25] Understanding the electronic structural change under potential and light, especially during the process of PEC, can be an important step toward gaining a mechanistic understanding of the new emerging catalyst/semiconductor interface. This makes the present work different from the previous works.[7-21] To the best of our knowledge, this study is the first report combining the studies of PEC performance of a CoB_i modified hematite nanorod array photoanode and *in situ* XAS at the Co K-edge.

Experimental

Chemicals. $Co(NO_3)_2$ (99.999%), boric acid (99.5%) and NaOH (>98%) are purchased from Sigma-Aldrich. 0.1 M sodium borate buffer (NaB_i, pH=9.2) is prepared by adding NaOH hydroxide pellets to boric acid solution. All electrolytes are prepared with DI water (18.6 MΩ.cm). FTO/glass (~7 Ω/sq) substrates are purchased from Sigma-Aldrich.

Photoelectrodeposition of CoBi on hematite photoanode. All electrochemical experiments for deposition and XAS measurements are performed using a CHI6016E working station (CHI Instruments) or an EmStat3+ (PalmSens) or EG&G Princeton Applied Research 273A potentiostat in a three-electrode system with the hematite/FTO substrates as working electrode, an Ag/AgCl reference electrode and a platinum wire counter electrode inside a home-made electrochemical cells. The preparation method for the hematite film can be found in our previous works.[19,21] All electrode potentials are converted to the reversible hydrogen electrode (RHE) scale. CoB_i is photoelectrodeposited on the hematite photoanode from a freshly prepared nitrogen purged 0.1 M borate buffer (pH = 9.2) solution containing 0.5 mM $Co(NO_3)_2$.[25] Photoelectrodeposition is carried out at 1.03 V for 10-20 min under a simulated visible light. The thickness of CoB_i is around 100 nm. After CoB_i deposition, the photoanode is rinsed with DI water and loaded immediately to the cell for XAS measurements. For short time storage, we immerse the film in NaB_i solution.

Characterization. The morphology of the photoanodes is characterized by FESEM (LEO Gemini 1530). X-ray diffraction (XRD) pattern measurements are carried out using a Bruker D8-Advance thin film X-ray diffractometer with a Cu Kα radiation (λ=0.154nm) at 40 kV and 40 mA. PEC measurements are performed in a three-electrode configuration in a home-made quartz-windowed Teflon cell. An Ag/AgCl reference electrode and a platinum counter electrode are used. AM1.5 solar illumination (100 $mWcm^{-2}$) provided by a WACOM solar simulator (WXS-50S-5H, class AAA) or Newport 96000 solar simulator is used to illuminate the sample. *In situ* XAS measurements in fluorescence mode (detector: Bruker X-Flash 6|60) are performed on a home-made cell (see Fig. S1) with a white LED (LEDWE-15, Thorlabs) illumination attached to the endstation at the KMC2 beamline at the BESSY II synchrotron in Berlin. The energy resolution of the beamline is 1/4000. The acquisition time for one XANES scan takes around 40 min. The beam size is around 250 mm x 600 mm (hor. x vert.). The electrolyte used for all measurements is

0.1 M NaB_i solution. Two Teflon sheets (~125 µm) are used as spacer to control the gap of the polymer window and the hematite photoanode. Using this configuration, it is possible to test semiconductor on FTO/glass substrate. The light intensity of the LED used for the *in situ* XAS measurements differs from the AM1.5 of the solar simulator for the PEC tests. The energy calibration is done using a cobalt foil. IPCE analysis is performed using the 300 W Xe lamp coupled into a grating monochromator (Acton SpectraPro 150i). The intensity of light is measured before IPCE measurements with a photodiode detector (Ophir PD300-UV). Electrochemical impedance spectroscopy (EIS) is performed in the dark at various frequencies between 0.1 Hz and 100 kHz. The X-ray photoelectron spectroscopy (XPS) measurements are carried out in an ultrahigh vacuum hemispherical XPS analyzer (SPECS PHOIBOS 100) and with a monochromatic X-ray source (SPECS FOCUS 500 monochromator, Al Kα radiation, 1486.74 eV).

Results and discussion

Morphology, Composition and Phase Study. The top view SEM images of the pristine and CoB_i modified hematite films are shown in Fig. 1. The hematite nanorod array photoanodes are prepared by a two-step method: hydrothermal synthesis of FeOOH and post-annealing.[19,21] A porous hematite nanorod array nanostructure is chosen in order to increase the surface area and compensate the short hole diffusion length (2 – 4 nm) of hematite.[6] It can be seen that the diameter and length of the nanorods is around 50 nm and 500 nm (see Fig. 1a inset). After CoB_i photoelectrodeposition, the hematite nanorods are covered by a layer of amorphous CoB_i film and no nanorods can be observed (see Fig. 1b and S2). The CoB_i/hematite film contains many cracks which are formed upon dehydration of the CoB_i film during SEM test and spherical particles with size ranging from a few hundreds of nanometers to µm-sized on the surface of the film (see Fig. 1b). Esswein *et al.*[11] and Surendranath *et al.*[26] previously reported on a CoB_i film containing µm-sized particles. Energy-dispersive X-ray spectroscopy (EDX) studies further confirm the deposition of CoB_i OEC on the hematite electrode (Fig. S3). EDX maps of the films shows uniform cobalt coverage on the hematite (Fig. S3a). The presence of boron is confirmed via X-ray photoelectron spectroscopy (XPS) (see Fig. S3c). XRD studies show that after CoB_i deposition, no additional peaks appear compared to bare hematite (see Fig. S4) except a broad hump at around 16°. This implies that the CoB_i film on hematite is amorphous. This is consistent with previous studies.[26,27]

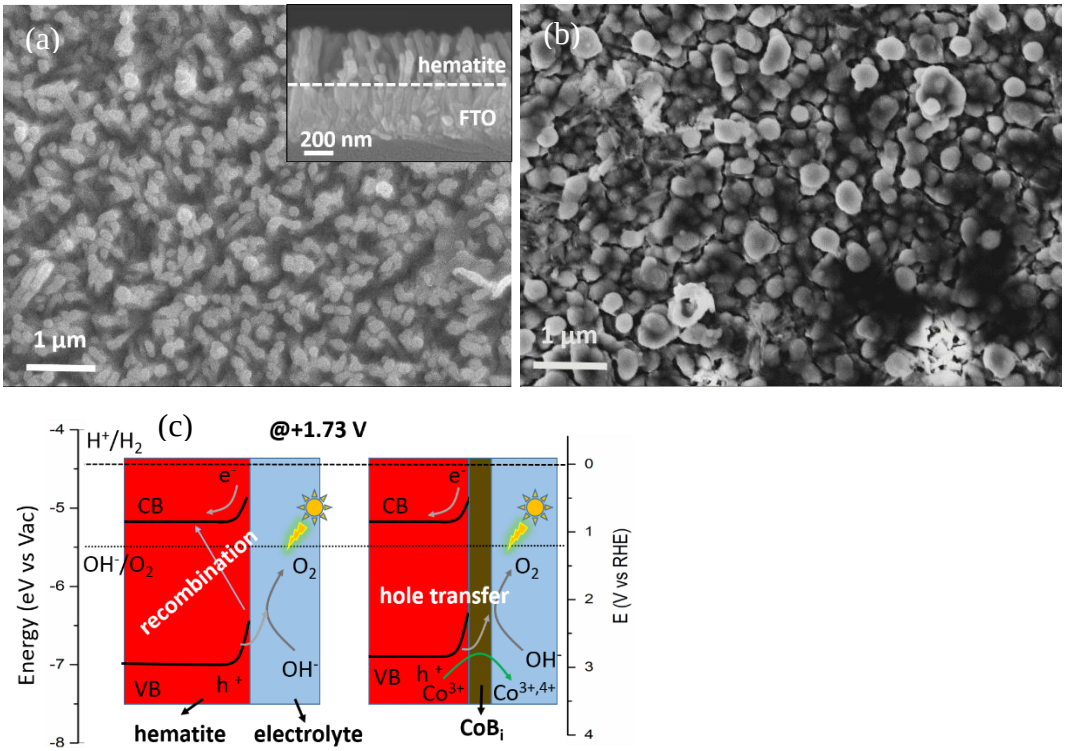

Fig. 1. SEM images of (a) the pristine (inset: cross-section image) and (b) the CoB_i modified hematite photoanode. (c) A schematic illustration of the effect of CoB_i modification.

PEC Performance. Fig. 2a shows photocurrent-potential (I-V) curves of the pristine hematite and of hematite modified with CoB_i under dark (dotted lines) and light (solid lines) conditions. It is found that CoB_i modification strongly affects the I-V characteristics. The photocurrent densities increase from 0.88 mA/cm^2 for the pristine nanorods to 1.12 mA/cm^2 at 1.23 V vs RHE after CoB_i modification, which is an increase of 27%. In this study, the potentials used are referring to RHE. It is worth mentioning that the photocurrent density improvement is more obvious for lower potentials. For example, at 1.0 V, the photocurrent density increases from 0.32 mA/cm^2 for the pristine hematite photoanode to 0.52 mA/cm^2 for the CoB_i modified one, which corresponds to an increase of 63%. The relatively low photocurrent density at low potential indicates a high electron-hole recombination rate. CoB_i modification also results in a negative shift (50 mV) of the photocurrent onset potentials. It can also be seen that the plateau of the CoB_i modified photoanode is broader, which provides good evidence for the cocatalyst modification.[11] We also deposit CoB_i on FTO/glass substrate and compare the CV curves of CoBi/FTO vs CoB_i modified hematite (see Fig. S5a). The CV curves clearly show the effect of CoB_i modification on the hematite photoanode. The light and potential effect can also be observed in the *I*–t curves obtained from measurements

in the *in situ* X-ray absorption near edge fine structure (XANES) cell (see Fig. S6a-b). The photocurrent improvements are further verified by measuring the photoanode IPCE at 1.23 V vs RHE as a function of the wavelength of the incident light (see Fig 2b). It can be seen that the CoB_i modified hematite which exhibits a similar response range, show slightly enhanced IPCE values compared to the pristine one. This indicates an efficient electron/hole pair separation and is consistent with their I-V characteristics. The IPCE drops substantially at wavelengths longer than 610 nm, as expected from the measurements of the hematite band gap.[6] The IPCE is 32 % at 350 nm for the CoB_i modified sample while that of the pristine samples is 20%. This further strengthens the argument that cocatalyst modification is important for improving the photoelectrochemical efficiency of hematite. The stability test results for bare and CoB_i modified hematite photoanodes are shown in Fig. S6c. It can be seen that both, the bare and the CoB_i modified hematite photoanodes, are relative stable under illumination and external potential.

In order to study the effect of CoB_i modification on the electronic properties of hematite in an electrolyte solution, electrochemical impedance spectroscopy (EIS) measurements are carried out. Fig. S5b shows the Nyquist plots of pristine and CoB_i modified hematite photoanodes at 1.0 V under dark conditions. It can be seen that the curve of the CoB_i modified hematite photoanode has a smaller radius compared to that of the pristine one. The diameter in Nyquist plots relates to the charge transfer resistance and the smaller diameter for the CoB_i modified hematite photoanode indicates faster charge transfer kinetics at the electrode interface. From the Mott-Schottky plots (see Fig. S5c), we can get nearly the same slope and the flat band potential (V_{FB}) regardless of the modification, which is comparable to previously reported values for hematite films.[21] Therefore, we conclude that CoB_i modification promotes the charge separation and water oxidation reaction on the surface of the hematite photoanode. All these factors lead to an increase of the photocurrents and to a negative shift of the photocurrent onset potentials (see Fig. 1c for a schematic illustration).

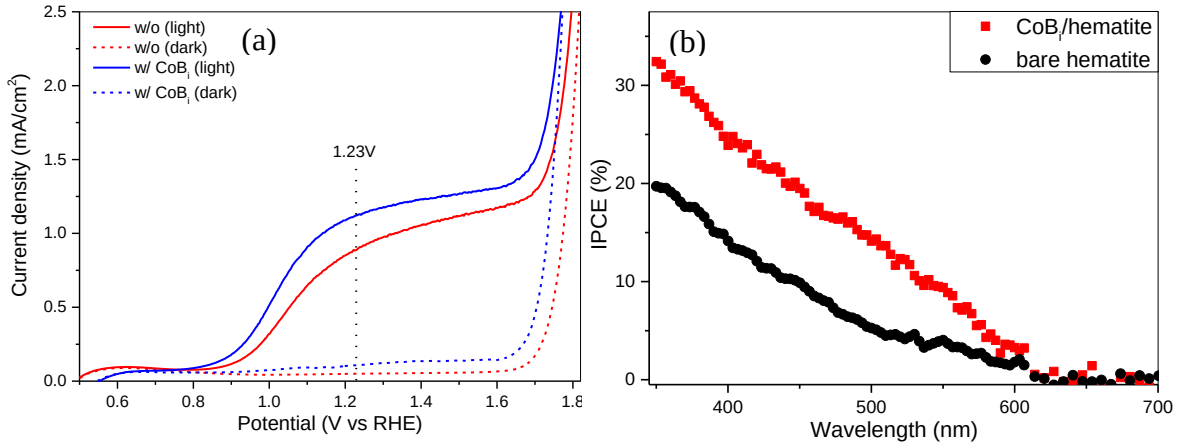

Fig. 2. (a) Photocurrent–potential (I–V) curves of a hematite photoanode with and without CoB_i modification under AM1.5 illumination in 0.1 M NaB_i solution. (b) IPCE spectra of a hematite photoanode with and without CoB_i modification.

Fig. 3 shows the X-ray photoelectron spectroscopy (XPS) spectra of the O 1s and Co 2p3/2 scans of the pristine and the CoB_i modified hematite photoanodes as deposited and after PEC test, respectively. In the O 1s core spectrum of the pristine hematite (see Fig. 3a), the features at binding energies of 529.9 and 531.0 eV correspond to the lattice O^{2-} (Fe-oxo bonds) and the lattice oxygen in a defective oxide environment,[28] respectively. The feature at 532.2 eV is assigned to the presence of a small amount of hydroxyl species and/or water[29-31] absorbed on the surface of the pristine hematite. By CoB_i modification, the O 1s spectrum changes. The lattice O^{2-} peak located at 529.9 eV slightly decreases in intensity, but the peaks located at 530.8 and 532.2 eV increase in intensity. The strong feature at 530.8 eV corresponds to the lattice O^{2-} (Co-oxo bonds in CoB_i). This implies that CoB_i contains a big portion of defect structure. The increased in intensity from the feature at 532.2 eV which corresponds to hydroxyl species and/or absorbed water implies that the amount of hydroxyl bonds in CoB_i/hematite as deposited or after PEC is larger than that of in the pristine hematite. This is consistent with the reported structure of CoB_i by Farrow *et al.*[22] In that study, using X-ray pair distribution function (PDF) analysis, they found that CoP_i and CoB_i have a Co oxyhydroxide (CoOOH) structure, but with diminished coherence in the stacking direction. After PEC test, the feature at 532.2 eV significantly increases and becomes dominant compared to the as deposited one. This can be due to an increase of surface hydroxyls species or a further disordered CoB_i structure, likely by intercalating water molecules between the layered CoOOH structures. This suggest that water in CoB_i is mostly chemisorbed or structurally bound. Note that the presence

of physisorbed water would instead lead to a shift of ~3 eV relative to the lattice O^{2-} peak and that physisorbed water is likely to dehydrate under UHV conditions.[28] As seen from Fig. 3b, the Co species in the as deposited CoB_i/hematite film are dominantly Co^{3+} (780.2 eV) and to a smaller extend Co^{2+} (781.2 eV).[32] The peak at 781.2 eV corresponds to a Co hydroxyl structure while the peak at 780.2 eV corresponds to a Co oxyhydroxyl structure. After PEC test, the peak intensity of the Co^{2+} species decreases (see the arrow in Fig. 3b), indicating the oxidation of a portion of Co^{2+} to Co^{3}, thus an increase of the average oxidation state. We do not observe Co^{4+} species from our XPS results and this stands in contrast to our XAS results determining the average oxidation state, which will be presented in next section. The possible reason is that these species may exist only under in situ conditions and are unstable in contact to air or UHV. This further strengthens the importance of *in situ* spectroscopy characterization of catalysts.

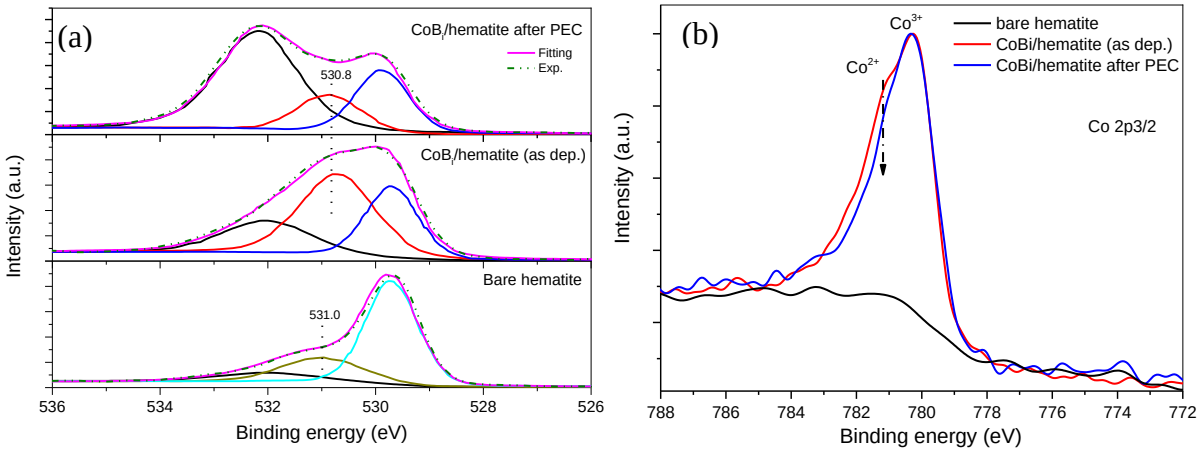

Fig. 3. (a) XPS spectra of (a) fitted O 1s spectra and (b) Co $2p_{3/2}$ spectra for the pristine and CoB_i modified hematite photoanode.

***In situ* XANES study.** Fig. 4a shows the XANES spectra of CoB_i/hematite along with Co reference oxides and CoB_i/FTO. Using the integral method,[33] the edge position of CoO is determined to be located at 7716.4 eV, of Co_3O_4 at 7719.1 eV and of $LiCoO_2$ at 7720.82 eV. The edge position of CoO_2 is obtained from Koyama's work.[34] For energy calibration the spectrum of the layered-rocksalt $LiCoO_2$ is used. Using a quantitative analysis method, a calibration curve is obtained using the reference compounds of Co (2+), Co (2.6+), Co (3+), and Co (4+) (see Fig. 4b). From this calibration curve, an increase of about 4.0 eV per cobalt oxidation state is obtained. Based on this calibration the calculated mean oxidation state of Co ions in CoB_i/FTO at OCP is 2.89 which is similar to that of previously reported CoP_i films by Kanan *et al.* (> 3.0)[35] and Risch *et al.* (~3.0).[36,37] However, we found that the cobalt catalyst deposited on hematite shows a higher

mean oxidation state at OCP condition. The calculated mean oxidation state of Co ions in CoB_i modified hematite at OCP is 3.38 (see Fig. S7a). A possible reason for the higher mean oxidation state for the CoB_i cocatalyst is that during the photoelectrodeposition process, Co ions in the CoB_i film are photo-oxidized to higher oxidation states by holes and the built-in potential generated from hematite. This process may also chemically passivate surface traps. It is proposed that the cobalt oxide catalyst becomes an active water oxidation catalyst when the mean oxidation state of Co is raised above 3.[35] These results suggest that the high catalytic activity of CoB_i on the surface of hematite may originate from the molecular structure of the component Co-oxo/hydroxo clusters.[36] Interestingly, when the potential is raised from OCP to 1.73 V (which is above the water oxidation onset potential), the mean oxidation state of CoB_i on FTO increases by 0.91 to 3.80, while that of CoB_i/hematite photoanode under dark and light conditions increase by 0.21 or 0.20 from 3.38 to 3.59 or 3.58, respectively (see Fig. 4b). The relative small change in mean oxidation state from CoB_i/hematite photoanode compared to CoB_i/FTO may be due to a higher resistance in the hematite film or charge recombination occurring at the surface of hematite. A relatively high oxidation state implies the presence of a large portion of Co^{4+} in the CoB_i film. Risch *et al.* previously observed that the calculated mean oxidation states of CoP_i vary from 2.60 ± 0.10 at low potential (0.95 V vs NHE) to 3.25 ± 0.10 at higher potential (1.49 V vs NHE).[38] The mean oxidation state difference is around 0.63 for their case. The possible reason for the smaller oxidation state difference is that the potential difference in their study is also smaller than in the here presented work.

In order to determine the fraction of different Co oxidation states in the CoB_i film, we assumed that the amount of Co (2+) is negligible[37] so that the mean oxidation state of 3.38 translates into populations of 62% Co (3+) and 38% Co (4+). For the CoB_i cocatalyst the mean oxidation state is around 3.59 at 1.73 V resulting in fractions of 42% Co (3+) and 58% of Co (4+). However, the fraction of Co (2+) in the freshly prepared film or film under low potential may be underestimated. Accordingly, the Co (4+) in the film under high potential may be underestimated if Co (2+) and Co (4+) coexist in the CoB_i cocatalyst.[38]

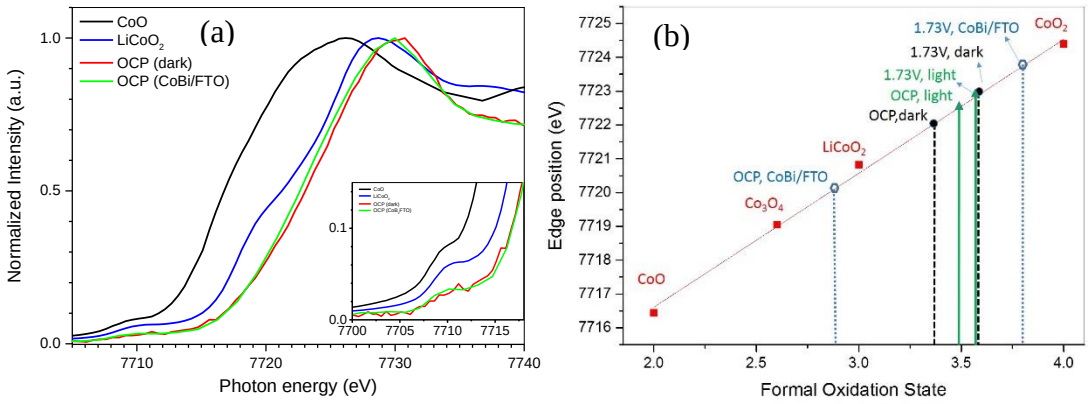

Fig. 4. Normalized XANES spectra of the cobalt K-edge of (a) CoB_i/hematite compared with cobalt oxides: CoO (2+) and $LiCoO_2$ (3+) and CoB_i deposited on a FTO/glass substrate. Inset: the magnified pre-edge region. (b) Edge positions obtained by the integral method. Black circles and green triangles show the edge position and mean oxidation state of the CoB_i/hematite under dark and light illumination, respectively. Blue open hexagons indicate the edge position and mean oxidation state of a CoB_i/FTO film.

A few reports pointed out the difficulty in determining metal valency based only on XANES spectra due to their sensitivity to geometry and ligand environment.[34,35,38] We also noted that in the literature, there is some controversy about the edge energy difference between CoO and Co cocatalysts. The edge position of CoB_i/hematite under dark conditions obtained from four estimation methods (max intensity, half height, inflection point and integral) is shown in Fig. S7b. We found that in general, the edge position changes under different potentials show a similar trend for all four methods. The edge position shifts to a higher energy when higher potential is applied. We found that the integral and half height methods give comparable values and thus appear to be the more reliable ones. Using the inflection point and the maximum intensity methods leads to different results and, although they are fast and easier, are therefore not recommendable. In this study, we will thus focus on the integral method.

Fig. 5 shows the effect of the applied potential and illumination conditions. In the dark, the CoBi/hematite film is oxidized with increasing potential (see Fig. 4b). Under illumination (see Fig 5b), the cobalt oxidation process requires less applied potential for oxidation compared to the film under dark conditions (see Fig 5a). The spectrum of CoB_i at OCP under illumination is shifted to higher energies compared to the one under dark conditions. The mean oxidation state of CoB_i/hematite at OCP in light is around 3.49 while it is 3.38 under dark conditions (see Fig 5c). The mean oxidation state thus increases. This means that at OCP conditions, photo-generated holes

oxidize CoB_i even without any external potential. We observed a similar phenomenon for a MnO_x modified $BiVO_4$ photoanode.[39] At higher potential, i.e. 1.13 V, a further upward band bending occurs at the CoB_i/hematite/electrolyte interface compared to at OCP condition. This promotes charge separation and provides the driving force for the migration of photogenerated holes toward the CoB_i layer. However, water oxidation does not occur at this potential; the majority of the photogenerated carriers will either accumulate and flatten the band, or recombine. When applying potential of 1.43 V or higher which is sufficient for water oxidation, a further upward band bending at the CoB_i/hematite interface occurs. It greatly promotes charge separation and reduces the charge recombination. The holes accumulated at the interface of CoB_i do not only oxidize Co but also oxidize water. When the film is gradually activated, likely after CoBi became disordered CoOOH layered structure, most of holes probably go to oxidize water (see Fig. 1c). This is consistent with the shift of edge position to higher energy as seen in Fig. 5c. After CoB_i modification, the recombination at the surface of hematite is probably greatly reduced. This is consistent with our PEC performance enhancement as shown in Fig. 2.

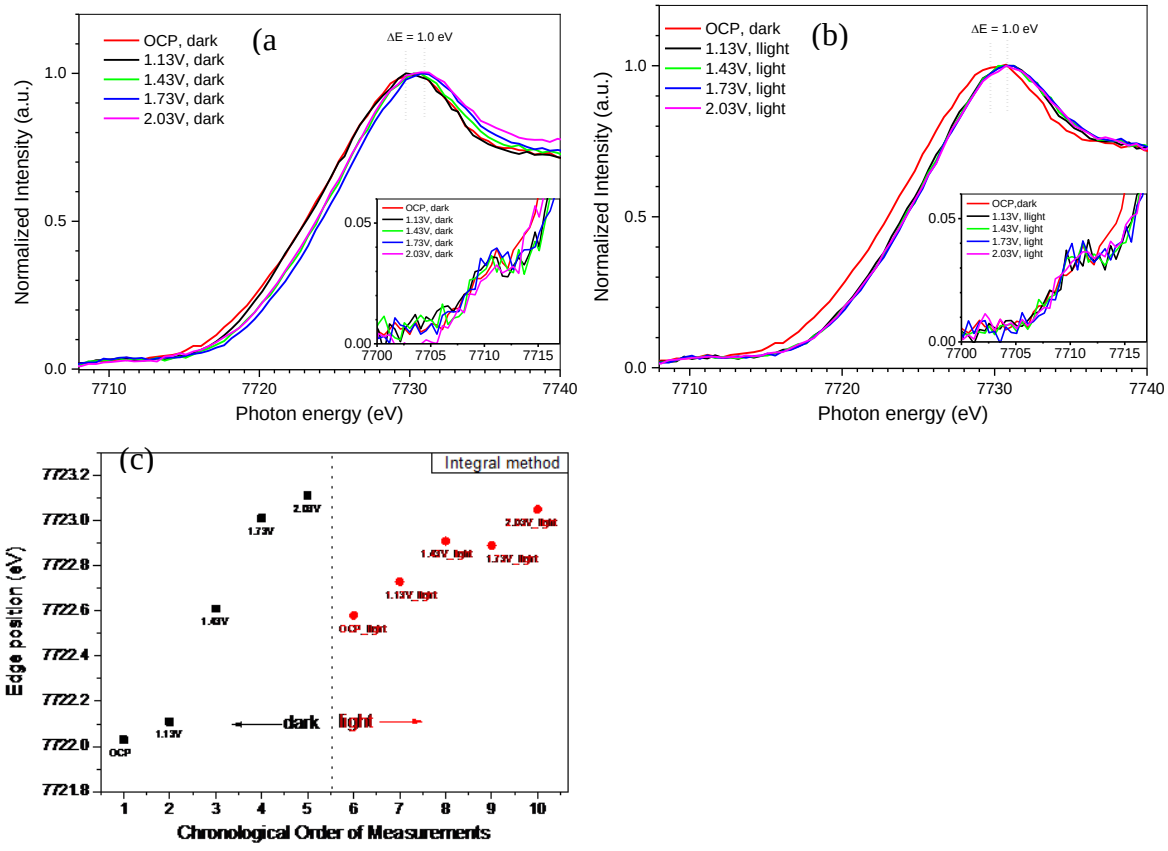

Fig. 5. Normalized XANES spectra at cobalt K-edge of CoB_i/hematite under different potentials (a) under dark and (b) in light. (c) Edge positions of CoB_i/hematite under different light conditions obtained by an integral method reported by Dau et al.[33]

Conclusions

In this study, we demonstrated that the PEC performance of a hematite photoanode can be improved by CoB_i modification. The current density at 1.23 V of the pristine hematite is 0.88 mA cm^{-2} and increased to 1.12 mA cm^{-2} after CoB_i modification (~27% improvement). The IPCE is 32 % at 350 nm for the CoB_i modified sample while that of the pristine one is 20%. The CoB_i cocatalayst layer is proposed to mainly improve OER kinetics and also prevent electron-hole recombination at the surface, thus improving the photocurrents and resulting in a negative shift of photocurrent onset potentials. These effects of CoB_i modification are supported by experimental data obtained by EIS, PEC and IPCE measurements. Nyquist plots show that the CoB_i-modified hematite photoanode has faster charge transfer kinetics at the electrode interface. To further investigate the electronic structure of a CoB_i cocatalyst deposited on hematite, *ex situ* XPS and *in situ* X-ray absorption spectroscopies are employed. *Ex situ* XPS O 1s spectra show that the amount of hydroxyl bonds in CoB_i/hematite as deposited or after PEC is larger than that of in the pristine hematite. *Ex situ* XPS test do not reveal the presence of Co^{4+} and this stands in contrast to our in situ XAS results determining the average oxidation state. The possible reason is that these species may exist only under in situ conditions and are unstable in contact to air or UHV. This further strengthens the importance of *in situ* spectroscopy characterization of catalysts. From *in situ* XAS test, the Co K-edge spectra under different potentials and illumination conditions were recorded. Using a quantitative analysis method, the information on the mean oxidation state of Co in the CoB_i film as well as the percentage of different Co species in the film under applied potential and illumination were revealed. We found that the mean oxidation state of Co ions in a CoB_i modified hematite photoanode is 3.38 which is higher than previous studies. A possible explanation for this may be the gradual photo-oxidation of the Co ions in the CoB_i during the photoelectrodeposition process. This process may also chemically passivate surface traps. We found that at OCP condition, light induced holes can oxidize the CoB_i film even without an external potential. With increasing potential the mean oxidation state of the CoB_i layer also increases which results from the photogenerated holes gradually oxidized Co ions into higher oxidation state, eg. Co (4+) in

CoB_i layer. However, this information cannot be revealed by *ex situ* XPS. We also compared different edge position determination methods and found that the integral method and half height methods are better. Using the inflection point and the maximum intensity methods is not recommended. The present work should benefit the potential application of OER catalyst on photoanodes and also strengthens the importance of *in situ* spectroscopy when studying catalysts.

Acknowledgments

We thank Dr I. Zizak, Dr G. Schuck, Mr J. Chen, Ms K. Chen for their assistance during the beamtime. We thank C. Höhn and P. Plate for their help in XPS test and data analysis. This work was supported by the Helmholtz Association (VH-NG-1140).

References

1. M. G. Walter, E. L. Warren, J. R. McKone, S. W. Boettcher, Q. Mi, E. A. Santori and N. S. Lewis, *Chem. Rev*. 2010, **110**, 6446-6473.
2. J. H. Yang, D. G. Wang, H. X. Han and C. Li, *Acc. Chem. Res.* 2013, **46**, 900-1909.
3. K. Sivula, F. Le Formal and M. Gratzel, *ChemSusChem*, 2011, **4**, 432-449.
4. A. B. Murphy, P. R. F. Barnes, L. K. Randeniya, I. C. Plumb, I. E. Grey, M. D. Horne and J. A. Glasscock, *Int. J. Hydrogen Energy*, 2006, **31**, 1999-2017.
5. F. Le Formal, N. Tetreault, M. Cornuz, T. Modehl, M. Gratzel and K. Sivula, *Chem. Sci.* 2011, **2,** 737-743.
6. Y. Ling, G. Wang, D. A. Wheeler, J. Z. Zhang and Y. Li, *Nano Lett.* 2011, **11**, 2119-2125.
7. Y. Qiu, S.-F. Leung, Q. Zhang, B. Hua, Q. Lin, Z. Wei, K.-H. Tsui, Y. Zhang, S. Yang and Z. Fan, *Nano Lett*. 2014, **14**, 2123–2129.
8. X. Wang, K. Peng, Y. Hu, F. Zhang, B. Hu, L. Li, M. Wang, X. Meng and S. Lee, *Nano Lett.* 2014, **14**, 18-23.
9. F. Lin and S. W. Boettcher, *Nature Mater.* 2014, **13**, 81-86.
10. M. Barroso, C. A. Mesa, S. R. Pendlebury, A. J. Cowan, T. Hisatomi, K. Sivula, M. Grätzel, D. R. Klug and J. R. Durrant, *Proc. Natl. Acad. Sci. U. S. A.*, 2012, **109**, 15640-15645.

11. D. K. Zhong, M. Cornuz, K. Sivula, M. Gratzel and D. R. Gamelin, *Energy Environ. Sci.*, 2011, **4**, 1759-1764.
12. G. M. Carroll and D. R. Gamelin, *J. Mater. Chem. A*, 2016, **4**, 2986-2994.
13. Y.-R. Hong, Z. Liu, S. F. B. S. A. Al-Bukhari, C. J. J. Lee, D. L. Yung, D. Chi and T. S. A. Hor, *Chem. Commun*., 2011, **47**, 10653-10655.
14. Z. Wang, G. Liu, C. Ding, Z. Chen, F. Zhang, J. Shi and C. Li, *J. Phys. Chem. C*, 2015, **119**, 19607-19612.
15. S. D. Tilley, M. Cornuz, K. Sivula and M. Grätzel, *Angew. Chem., Int. Ed.*, 2010, **122**, 6549-6552.
16. X. Chen, X. Ren, Z. Liu, L. Zhuang and J. Lu, *Electrochem. Commun.* 2013, **27**,148-151.
17. A. G. Tamirat, J. Rick, A. A. Dubale, W.-N. Su and B.-J. Hwang, *Nanoscale Horiz.*, 2016, **1**, 243-267.
18. E. Thimsen, F. Leformal, M. Grätzel and S. C. Warren, *Nano Lett.* 2011, **11**, 35–43.
19. L. Xi, P. D. Tran, S. Y. Chiam, P. S. Bassi, W. F. Mak, H. K. Mulmudi, S. K. Batabyal, J. Barber, J. S. C. Loo and L. H. Wong, *J. Phys. Chem. C*, 2012, **116**, 13884-13889.
20. L. Xi, P. S. Bassi, S. Y. Chiam, W. F. Mak, P. D. Tran, J. Barber, J. S. Chye Loo and L. H. Wong, *Nanoscale*, 2012, **4**, 4430-4433.
21. L. Xi, S. Y. Chiam, W. F. Mak, P. D. Tran, J. Barber, S. C. J. Loo and L. H. Wong, *Chem. Sci*., 2013, **4**, 164-169.
22. C. L. Farrow, D. K. Bediako, Y. Surendranath, D. G. Nocera and S. J. Billinge, *J. Am. Chem. Soc*., 2013, **135**, 6403-6406.
23. H. Kurosu, M. Yoshida, Y. Mitsutomi, S. Onishi, H. Abe and H. Kondoh, *Electrochemistry*, 2016, **84**, 779-783.
24. J. Yano and V. K. Yachandra, *Photosynth. Res*., 2009, **102**, 241-254.
25. A. J. Esswein, Y. Surendranath, S. Y. Reece and D. G. Nocera, *Energy Environ. Sci*., 2011, **4**, 499-504.
26. Y. Surendranath, M. Dinca and D. G. Nocera, *J. Am. Chem. Soc*., 2009,**131**, 2615-2620.
27. R. L. Doyle, I. J. Godwin, M. P. Brandon and M. E. G. Lyons, *Phys. Chem. Chem. Phys*., 2013, **15**, 13737-13783.
28. I. V. Chernyshova, S. Ponnurangam and P. Somasundaran, *Phys. Chem. Chem. Phys.*, 2013, **15**, 6953-6964.

29. K. K. Lee, *"Studies of cobalt and iron oxides/oxyhydroxides nanostructures for electrochemical applications"*, PhD thesis, National University of Singapore, Singapore, 2013.
30. B, Liu, H-Q. Peng, C-N. Ho, H. Xue, S. Wu, T-W. Ng, C-S. Lee and W. Zhang. *Small* 2017, 1701875.
31. O.M. Ivasishin, D.G. Savvakin, O.B. Bondarchuk, M.M. Gumenyak, role of surface containimation in titantium PM, *Key Eng. Mater.* 2012, **520**, 121-132.
32. H. Qin, X. Qian, T. Meng, Y. Lin and Z. Ma, *Catalysts*, 2015, **5**, 606-633.
33. H. Dau, P. Liebisch and M. Haumann, *Anal. Bioanal. Chem*., 2003, **376**, 562-583.
34. Y. Koyama, H. Arai, Z. Ogumi, I. Tanaka and Y. Uchimoto, *Phys. Rev. B: Condens. Matter Mater. Phys.*, 2012, **85**, 075129.
35. M. W. Kanan, J. Yano, Y. Surendranath, M. Dinca, V. K. Yachandra and D. G. Nocera, *J. Am. Chem. Soc.*, 2010, **132,** 13692-13701.
36. M. Risch, V. Khare, I. Zaharieva, L. Gerencser, P. Chernev and H. Dau, *J. Am. Chem. Soc*., 2009, **131**, 6936-6937.
37. M. Risch, D. Shevchenko, M. F. Anderlund, S. Styring, J. Heidkamp, K. M. Lange, A. Thapper and I. Zaharieva, *Int. J. Hydrogen Energy*, 2012, **37**, 8878-8888.
38. M. Risch, F. Ringleb, M. Kohlhoff, P. Bogdanoff, P. Chernev, I. Zaharieva and H. Dau, *Energy Environ. Sci*., 2015, **8**, 661-674.
39. L. Xi, F. Wang, C. Schwanke, F. F. Abdi, R. Golnak, S. Fiechter, K. Ellmer, R. van de Krol and K. M. Lange. *J. Phys. Chem. C*, 2017, **121**, 19668–19676.

Table of Content

The first report combines the studies of the PEC performance of CoB_i/hematite photoanode and *in situ* XAS at the Co K-edge.